The International Maritime Transport and Logistics (MARLOG 15) - ISSN 2974-3141
http://dx.doi.org/10.21622/MARLOG.2026.15.1.101
Smart & Resilient Logistics Corridors Future Gateway to the Green Trade

NUMERICAL INVESTIGATION OF OPERATIONAL DOWNTIME AT GARGOUB COMMERCIAL PORT

Youssef A. Abdrabou [1], Moataz S. Hassan [2] and Maysara K. El-Tahhan [2]

(1) Smart Environment and Climate Change Management MSc Student, Faculty of Science, Alexandria University, Alexandria, Egypt
(2) Transportation Engineering Department, Faculty of Engineering, Alexandria University, Alexandria, Egypt

Keywords: Gargoub Port, Operational Downtime, MIKE 21, Sea-Level Rise (SLR)

ABSTRACT

This study presents a comprehensive numerical assessment of operational downtime at Gargoub Commercial Port, a strategic Mediterranean development in Egypt, under current and projected climate conditions. Coastal ports are increasingly susceptible to wave-induced disturbances and sea- level rise (SLR). A 30-year offshore wave hindcast (1994–2024) was produced using a calibrated MIKE 21 Spectral Waves (SW) model, with the outputs informing simulations of wave behavior in the port basin using MIKE 21 Boussinesq Waves (BW) for two development layouts: the near-complete interim layout (Layout 1) and the final planned expansion (Layout 2). Operational downtime at Gargoub Port was assessed under current and projected SLR conditions following PIANC (2014) quay-specific thresholds. Under Layout 1, bulk carriers and general cargo vessels were largely unaffected under both the baseline and SLR conditions, whereas container and Ro-Ro vessels experienced notable downtime at the more exposed multi-purpose quays. Expansion of the port (Layout 2) eliminated wave-induced downtime for all vessel types, demonstrating enhanced operational resilience. A projected SLR of +1.01 m had a negligible effect on berth-level operations, and full port shutdown at the navigation channel remained nearly unchanged (341–345 hours/year). These findings highlight the importance of port configuration and offshore wave climate in shaping operational performance and demonstrate the applicability of the modeling framework for supporting resilient port planning and management in comparable coastal settings.

1. INTRODUCTION

With nearly 80% of global trade transported by sea, ports are critical nodes in international supply chains, supporting global economic activity and driving social, economic, and spatial development in their surrounding regions (Becker et al., 2013; Michel et al., 2024; Mamdouh et al., 2024). In recent years, Egypt's maritime ports have undergone substantial development, particularly between 2014 and 2025, as part of a national strategy to position the country as a regional transport and logistics hub (Maritime Transport & Logistics

Sector, Arab Republic of Egypt). However, ports located in low-lying coastal areas are inherently exposed to climate-related hazards such as SLR, storm surges, and extreme wave conditions, which can adversely affect vessel navigation, berthing, cargo handling, and terminal operations, ultimately leading to operational downtime and economic losses (Becker et al., 2013; Sierra et al., 2016; Romya et al., 2025).

Numerical hydrodynamic models have become essential tools for assessing port functionality under environmental forcing, enabling high-resolution simulation of waves and nearshore processes relevant to harbor design and operational management (Samaras et al., 2016; Al-Rammahi & Al-Shukur, 2025). Quay walls are essential port infrastructure that support vessel berthing and cargo handling operations,

and their design must account for operational and environmental conditions (Kamel et al., 2025). Recent studies increasingly rely on high-resolution, site-specific modeling to evaluate wave-induced harbor agitation and operational downtime under present and future conditions. For instance, investigations at Tangier-Med port in Morocco indicate that SLR reduces freeboard and increases downtime (Jebbad et al., 2022), while studies of Catalan and Balearic ports demonstrate that combined SLR and changing wave regimes can significantly compromise harbor functionality (Sierra et al., 2015, 2017, 2023; Romya et al., 2025). In several cases, wave-induced agitation has been shown to pose a greater operational constraint than SLR alone, highlighting the importance of detailed wave modeling for reliable downtime assessment (Romya et al., 2025).

Despite extensive research on major Mediterranean ports, Gargoub Port, currently under development, has not been previously assessed. The port presently supports small-scale maritime activities and is planned for expansion through new berths, cargo handling areas, and breakwaters (Maritime Transport & Logistics Sector, Arab Republic of Egypt, 2025), yet its operational downtime remains unquantified. To address this gap, the present study evaluates the current and projected operational downtime of Gargoub Port under present conditions and a SLR scenario by 2100 using the MIKE 21 Spectral Waves FM and MIKE 21 Boussinesq Waves modules.

2. STUDY AREA

Gargoub Port is located approximately 70 km west of Matrouh in the El Negaila region, at coordinates 26°33′ E and 31°29′ N (Figure 1). The port is undergoing expansion and comprises eight primary quay walls, five multipurpose, two general cargo, and one container quay, protected by a system of breakwaters, with an operational water depth of approximately 17 m along the quays. Quay lengths were obtained from the port's official website and are illustrated in Figure 1. For this study, two development layouts are considered, derived by combining official design data from the Maritime Transport Sector website with recent satellite imagery depicting the ongoing construction status. Layout 1 represents the near-completed stage, extending up to the indicated boundary in Figure 1, in which the Northern Breakwater has been constructed to approximately 3,050 m, together with an additional planned 3,500 m segment. Layout 2 corresponds to the final planned configuration, incorporating the revetment extension and the Northern Breakwater, which consists of the existing 3,050 m section and a new extension of approximately 5,300 m. These layouts are used to assess wave agitation and operational downtime under present and future sea-level conditions.

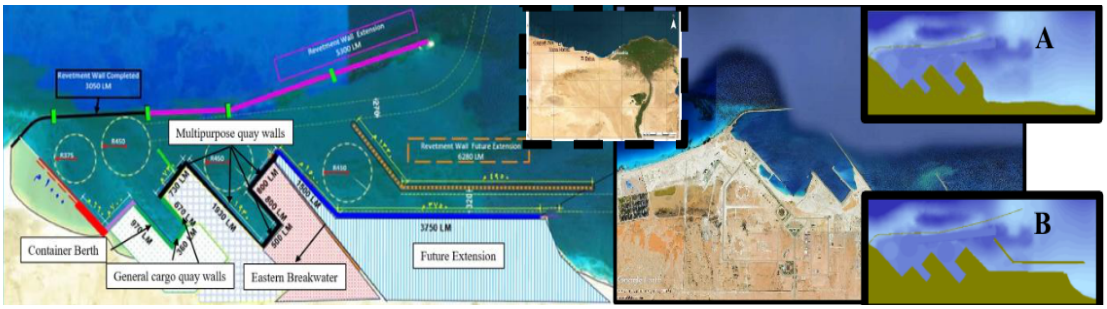

Figure 1. Gargoub Port study area showing the two development layouts: (A) Layout 1 (near-completed stage) and (B) Layout 2 (full planned configuration). (Maritime Transport & Logistics Sector, Arab Republic of

3. MATERIALS AND METHODS

3.1. Data Sources

Bathymetric data were obtained from the EMODnet Digital Bathymetry dataset with a spatial resolution of approximately 115 m. The offshore wave and wind climate was characterized using the ECMWF ERA5 global reanalysis, with metocean parameters, including significant wave height (Hs), peak wave period (Tp), mean wave direction (MWD), and 10-m wind speed (WS) and direction (WD), extracted for 1994–2024 at a boundary point (31°55′53.15″ N, 26°41′13.03″ E) to force the offshore boundary of the MIKE 21 Spectral Waves (SW) model (DHI, Denmark), propagating conditions to the nearshore zone. The SW model was calibrated and validated against the previously calibrated Northern Egyptian Wave Model (CoRI) (Romya et al., 2025) at two stations separated by ~18 km: Station 1 (31°42′45.13″ N, 26°37′23.77″ E) and Station 2 (31°33′30.36″ N, 26°34′43.08″ E). The year 2004 was selected for calibration due to the availability of high-quality, continuous observations used by Romya *et al.* to calibrate their model. Total water level data were obtained from CMEMS, corrected relative to mean sea level (MSL), and used to force the SW model over the period 1994–2024. For MIKE 21 Boussinesq Waves (BW) simulations, scenario-dependent constant water levels were applied to represent specific hydrodynamic states.

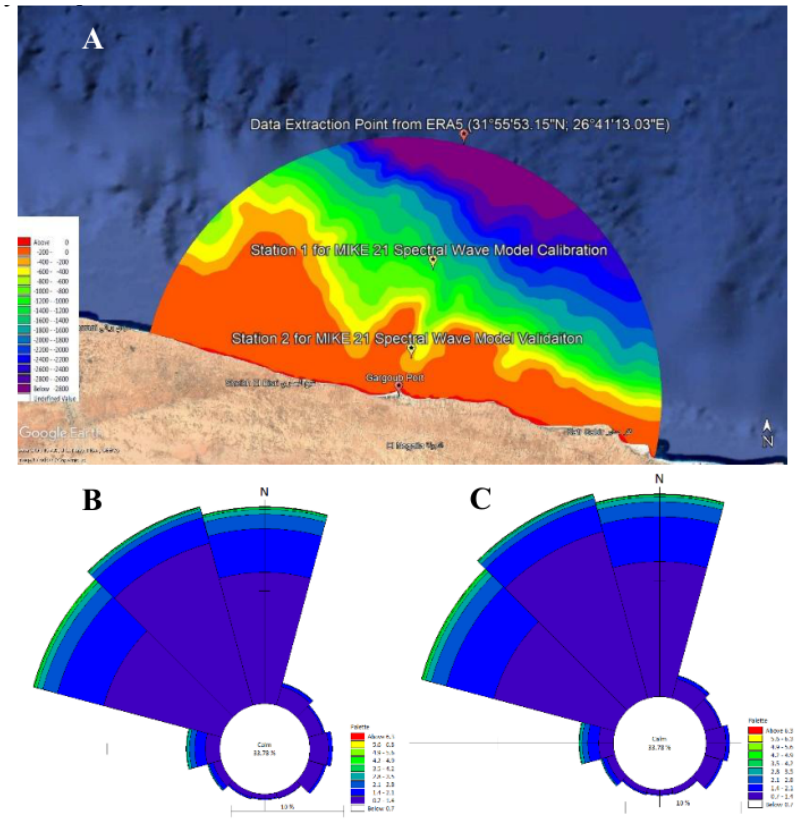

Figure 2. Model setup and offshore climate characterization for Gargoub Port. (A) The nested computational mesh for the MIKE 21 Spectral Waves (SW) model, indicating the offshore boundary (ERA5 forcing location) and the calibration/validation stations. (B) Wind rose derived from ERA5 data (1994–2024) at the offshore boundary point, showing the predominant wind regime. (C) Wave rose from the same ERA5 dataset, illustrating the statistical offshore wave climate.

3.2. MIKE 21 Spectral Waves (SW) Model

3.2.1. Model Setup

Wave transformation was simulated using the computationally efficient directionally decoupled parametric formulation, based on the moment-based parameterization of Holthuijsen *et al.* (1989) and recommended for domains of 10–50 km (DHI MIKE, 2025). A multi-level nested mesh system propagated waves from offshore to nearshore, with resolutions of 1000 × 1000 m (offshore), 300 × 300 m (intermediate), and 60 × 60 m (nearshore), totaling 41,105 elements to resolve shoaling, refraction, and nearshore transformation. The spectral wave (SW) model was run in two phases: calibration/validation during 2004, and the full 1994–2024 period to generate wave probability distributions for BW simulations. The northern offshore boundary was forced with ERA5 waves and wind fields along with CMEMS water levels.

3.2.2. Physical Parameterization and Calibration

Model calibration focused on bottom friction and ERA5 wind adjustments. Three bottom friction values, based on the median sediment diameter (d_{50}), were tested, along with several wind enhancements. Wind adjustments were considered because ERA5 is known to underestimate strong winds and extreme events, particularly during high-energy offshore

and coastal conditions (Gandoin & Garza, 2024; Alkhalidi et al., 2025; Ji et al., 2025). To address this limitation, different wind enhancements, by increasing wind speeds by 10% and 20%, were applied as part of the calibration improvement process. A summary of the SW calibration runs is shown below:

Table 1: Calibration runs of the spectral wave model, showing tested d50 values and applied wind enhancements to improve model performance.

Run	1	2	3	4	5
d50 (mm)	0.125	0.25	0.5	0.125	0.125
Wind Speed Increase (%)	0	0	0	10	20

Model accuracy was evaluated through a set of statistical performance metrics, namely the correlation coefficient (R), Root Mean Square Error (RMSE), Bias, and Scatter Index (SI). The corresponding equations employed to derive these parameters are provided below:

$$R = \frac{\sum_{i=1}^{N}\left((P_i - \bar{P})(M_i - \bar{M})\right)}{\sqrt{\sum_{i=1}^{N}(P_i - \bar{P})^2 \left(\sum_{i=1}^{N}(M_i - \bar{M})^2\right)}} \quad (1)$$

$$RMSE = \sqrt{\frac{1}{N}\sum_{i=1}^{N}(P_i - M_i)^2} \quad (2)$$

$$Bias = \sum_{i=1}^{N}\frac{1}{N}(P_i - M_i)^2 \quad (3)$$

$$SI = \frac{\sqrt{\frac{1}{N}\sum_{i=1}^{N}(P_i - M_i)^2}}{\bar{M}} \quad (4)$$

Where M_i is the measured value, $\bar{M}$ is the mean value of the measured data, P_i is the predicted value, $\bar{P}$ is the mean value of the predicted data and N is the number of data points.

3.3. MIKE 21 Boussinesq Waves (BW) Model

3.3.1. Domain and Forcing

Wave data extracted from the SW model at selected locations were used as boundary inputs for the BW model, representing wave generation points for the simulations. The BW model employed a 3 × 3 m grid to cover a 12 km × 4.6 km domain to resolve wave–structure interactions in the port basin. Each scenario applied a constant water level, representing either the maximum observed 2024 water level (baseline) or the baseline plus 1.01 m of SLR. Wave heights were obtained from the SW model at the wave generator locations for Layout 1 (31°30′23.29″ N, 26°37′24.97″ E) and Layout 2 (31°30′36.91″ N, 26°40′40.51″ E), with directional forcing of 30° ±30°. Representative porosity coefficients, defining the fraction of water flow through porous structures, were assigned to model boundaries using the MIKE 21 Toolbox based on structure type and local wave conditions. Values of 0.8 were used for the shoreline and 0.6 for rock slopes, while vertical quay walls were treated as fully reflective. Sponge layers of one to two wavelengths were applied at the domain boundaries to absorb outgoing energy and ensure numerical stability. (MIKE).

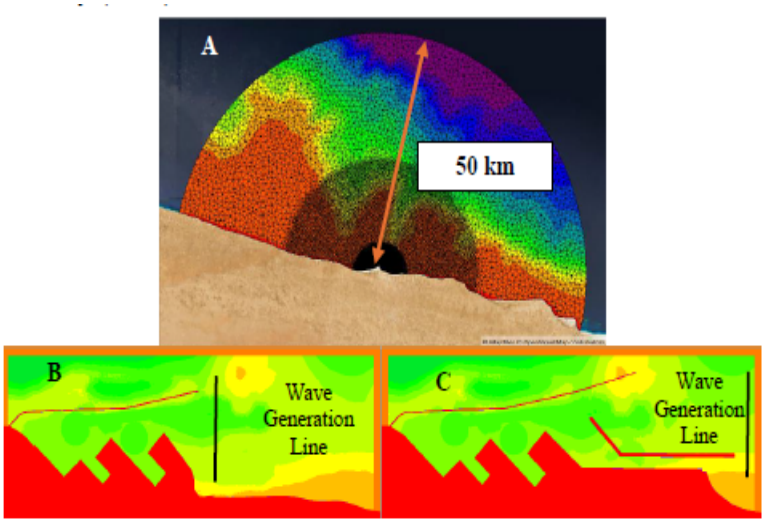

Figure 3. (A) Offshore, intermediate, and nearshore grids of the spectral wave (SW) model with resolutions of ~1000 m × 1000 m, ~300 m × 300 m, and ~60 m × 60 m, respectively. (B) Grid for the Boussinesq wave (BW) model for Layout 1 (current development stage) (C) Grid for Layout 2 (future development stage)

3.3.2. Modeled Scenarios

Table 2: Summary of tested scenarios by the BW waves module

Scenario	Layout	Characteristics	Water Level (m) (MSL)
1	1 (Figure 3B)	SLR not Considered	Highest Total Water Level (2024 record) = 0.3 m
2	1 (Figure 3B)	SLR Considered	Highest Total Water Level (2024 record) = 0.3 m + 1.01 m SLR
3	2 (Figure 3C)	SLR not Considered	Highest Total Water Level (2024 record) 0.3 m
4	2 (Figure 3C)	SLR Considered	Highest Total Water Level (2024 record) = 0.3 m + 1.01 m SLR

The +1.01 m SLR scenario represents the upper bound of the likely range for 2100 under the high- emission SSP5-8.5 pathway (IPCC). This robust, policy-relevant value is standard for engineering assessments, while more extreme (>2 m) low-likelihood outcomes are excluded. The scenario is further justified for the Egyptian coast by regional vulnerability studies. The Integrated Coastal Vulnerability Index (ICVI) classifies 70% of Egypt's Mediterranean shoreline as highly vulnerable, with peak values reaching 4.9 (Hzami et al., 2021). Thus, the +1.01 m scenario provides a conservative yet plausible benchmark for evaluating future operational risks at Gargoub Port.

3.4. Downtime Analysis

3.4.1. Criteria

Operational downtime was assessed by comparing simulated wave heights at each berth against the PIANC (2014) loading/unloading thresholds for their designated vessel types. For multi-purpose quay walls, this evaluation included container ships, Ro-Ro vessels, general cargo ships, and bulk carriers. Dedicated general cargo and container quays were assessed for their specific ship types. The analysis accounted for the critical transverse wave direction. In addition, full port shutdown was evaluated by analyzing wave heights at the navigation channel entrance using the SW model outputs and applying the 2.0 m exceedance threshold established by Egyptian port authorities (Romya et al., 2025). The annual operational downtime for each vessel type was quantified as the percentage of time the simulated wave heights exceeded the corresponding threshold.

4. RESULTS AND DISCUSSION

4.1. Spectral Wave Model Calibration and Validation

The SW model was calibrated against reference wave data from the CoRI Northern Egyptian Wave Model (Romya et al., 2025) for the year 2004. Statistical performance metrics including Correlation Coefficient (R), Root Mean Square Error (RMSE), Bias, and Scatter Index (SI) were calculated for two stations.

Table 3: Statistical performance of SW calibration runs.

Run	Wind speed increase (%)	d50 (mm)	Station 1: 31°42'45.13"N; 26°37'23.77"E				Station 2: 31°33'30.36"N; 26°34'43.08"E			
			RMSE (m)	Bias (m)	R	SI	RMSE (m)	Bias (m)	R	SI
1	0	0.125	0.1697	-0.0059	0.9699	0.1577	0.2198	-0.1661	0.8940	0.2191
2	0	0.25	0.1699	-0.0065	0.9699	0.1579	0.2208	-0.1693	0.8945	0.2200
3	0	0.5	0.1699	-0.0071	0.9698	0.1580	0.2212	-0.1719	0.8943	0.2205
4	10	0.125	0.1697	0.0059	0.9699	0.1577	0.2198	-0.1661	0.8940	0.2191

All calibration runs showed very high skill at offshore Station 1 (R ≈ 0.97, SI ≈ 0.16), confirming robust deep-water wave simulation. Performance at Station 2, subject to shallower bathymetry, remained strong (R > 0.89, SI ≈ 0.22). Runs 1 and 4 yielded identical

optimal statistics with the lowest RMSE and minimal bias, indicating wind generation was secondary to swell transformation. Run 5 (20% wind mark-up) was selected as the optimal configuration, retaining Run 1's excellent offshore metrics while slightly improving the nearshore correlation (R = 0.8943). These results confirm high model skill, and the wind enhancement provides a more physically realistic representation. Consequently, run 5 was used for the full scenario simulation (1994–2024).

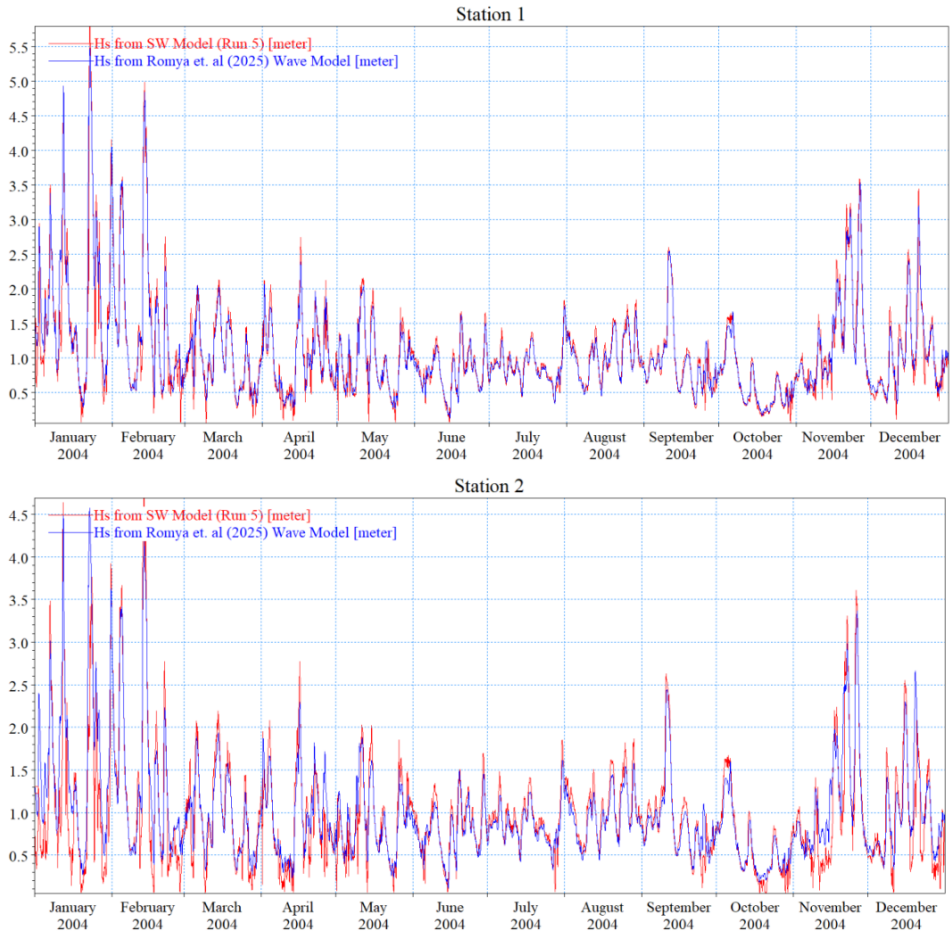

Figure 4. (A) Calibration of Hs at Station 1 (R ≈ 0.97, SI ≈ 0.16). (B) Validation of H at Station 2, (R > 0.89, SI ≈ 0.22).

4.2. Harbor Tranquility and Operational Downtime Analysis

4.2.1. Boussinesq Wave Model Setup and Methodology

The MIKE 21 Boussinesq Wave (BW) module was used to simulate wave activity within the port basin and assess berth operability, capturing non-linear processes such as shoaling, refraction, diffraction, and reflection. Wave forcing was derived from the validated SW model. A representative significant wave height (Hm0-incoming) of 1.0 m (mean direction 30°, spreading ±30°) was applied at the port entrance from the BW model's wave generator, representing the most critical wave approach, as the port is particularly vulnerable to eastern waves. Model outputs were expressed as the non-dimensional wave height ratio (Hm0/Hm0-incoming) at each assessment point, where Hm0-incoming corresponds to the wave height at the wave generator. This site-specific attenuation ratio was applied together with the long-term wave height probability distributions from two 30-

year SW model runs, one with current water depths and the other with depths deepened to account for projected sea level rise (SLR), to calculate the annual exceedance of PIANC operational thresholds at each quay wall under both conditions.

Table 4: Distribution of significant wave heights (Hs) at the wave generator for Layout 1 under (A) current water levels and (B) projected sea level rise (SLR), categorized by mean wave direction (MWD).

A

Hs (m)/MWD (°)	[0, 60)	[60, 120)	[120, 180)	[180, 240)	[240, 300)	[300, 360)	Total
[0.0, 0.5)	5.67	5.12	1.78	2.06	4.36	12.84	31.83
[0.5, 1.0)	12.66	0.17	0.00	0.00	0.20	32.30	45.33
[1.0, 1.5)	4.70	0.00	0.00	0.00	0.00	11.85	16.56
[1.5, 2.0)	1.36	0.00	0.00	0.00	0.00	2.90	4.26
[2.0, 2.5)	0.17	0.00	0.00	0.00	0.00	1.01	1.18
[2.5, 3.0)	0.00	0.00	0.00	0.00	0.00	0.60	0.60
[3.0, 3.5)	0.00	0.00	0.00	0.00	0.00	0.17	0.17
[3.5, 4.0)	0.00	0.00	0.00	0.00	0.00	0.07	0.07
[4.0, 4.5)	0.00	0.00	0.00	0.00	0.00	0.01	0.01
Total	24.56	5.29	1.78	2.06	4.56	61.74	100.00

B

Hs (m)/MWD (°)	[0, 60)	[60, 120)	[120, 180)	[180, 240)	[240, 300)	[300, 360)	Total
[0.0, 0.5)	4.94	5.10	1.88	2.17	4.74	11.72	30.55
[0.5, 1.0)	11.28	0.44	0.00	0.00	0.35	33.58	45.66
[1.0, 1.5)	4.67	0.00	0.00	0.00	0.00	12.28	16.94
[1.5, 2.0)	1.78	0.00	0.00	0.00	0.00	2.90	4.68
[2.0, 2.5)	0.32	0.00	0.00	0.00	0.00	0.97	1.28
[2.5, 3.0)	0.02	0.00	0.00	0.00	0.00	0.61	0.63
[3.0, 3.5)	0.00	0.00	0.00	0.00	0.00	0.16	0.16
[3.5, 4.0)	0.00	0.00	0.00	0.00	0.00	0.06	0.06
[4.0, 4.5)	0.00	0.00	0.00	0.00	0.00	0.02	0.02
Total	23.01	5.55	1.88	2.17	5.09	62.30	100.00

Table 5: Distribution of significant wave heights (Hs) at the wave generator for Layout 2 under (A) current water levels and (B) projected sea level rise (SLR), categorized by mean wave direction (MWD).

A

Hs (m)/MWD (°)	[0, 60)	[60, 120)	[120, 180)	[180, 240)	[240, 300)	[300, 360)	Total
[0.0, 0.5)	2.69	5.29	2.04	1.94	5.27	11.72	28.95
[0.5, 1.0)	4.77	1.33	0.00	0.00	1.20	39.97	47.27
[1.0, 1.5)	1.40	0.01	0.00	0.00	0.00	16.15	17.57
[1.5, 2.0)	0.29	0.00	0.00	0.00	0.00	3.62	3.91
[2.0, 2.5)	0.09	0.00	0.00	0.00	0.00	1.27	1.36
[2.5, 3.0)	0.01	0.00	0.00	0.00	0.00	0.63	0.64
[3.0, 3.5)	0.00	0.00	0.00	0.00	0.00	0.19	0.19
[3.5, 4.0)	0.00	0.00	0.00	0.00	0.00	0.08	0.08
[4.0, 4.5)	0.00	0.00	0.00	0.00	0.00	0.03	0.03
Total	9.24	6.64	2.04	1.94	6.47	73.67	100.00

B

Hs (m)/MWD (°)	[0, 60)	[60, 120)	[120, 180)	[180, 240)	[240, 300)	[300, 360)	Total
[0.0, 0.5)	2.69	5.06	2.23	2.04	5.06	10.56	27.64
[0.5, 1.0)	4.69	1.58	0.00	0.00	1.83	38.32	46.42
[1.0, 1.5)	1.53	0.03	0.00	0.00	0.01	17.48	19.05
[1.5, 2.0)	0.30	0.00	0.00	0.00	0.00	4.16	4.46
[2.0, 2.5)	0.09	0.00	0.00	0.00	0.00	1.37	1.46
[2.5, 3.0)	0.01	0.00	0.00	0.00	0.00	0.65	0.66
[3.0, 3.5)	0.00	0.00	0.00	0.00	0.00	0.21	0.21
[3.5, 4.0)	0.00	0.00	0.00	0.00	0.00	0.07	0.07
[4.0, 4.5)	0.00	0.00	0.00	0.00	0.00	0.03	0.03
Total	9.30	6.67	2.24	2.04	6.91	72.85	100.00

Four BW scenarios were simulated, corresponding to the two port layouts (Layout 1: near complete; Layout 2: final expansion) and two sea-level conditions (Baseline; Baseline + 1.01 m SLR), as defined in Table 2. Wave heights were extracted at 30 representative points along the quay walls (Figure 5). For each berth, the maximum simulated wave height was compared against the operational thresholds defined by PIANC (2014) for relevant vessel types (e.g., container ships, bulk carriers, general cargo). The percentage of time the simulated wave height exceeded the threshold was calculated to determine annual operational downtime, expressed in hours/year (hr/yr).

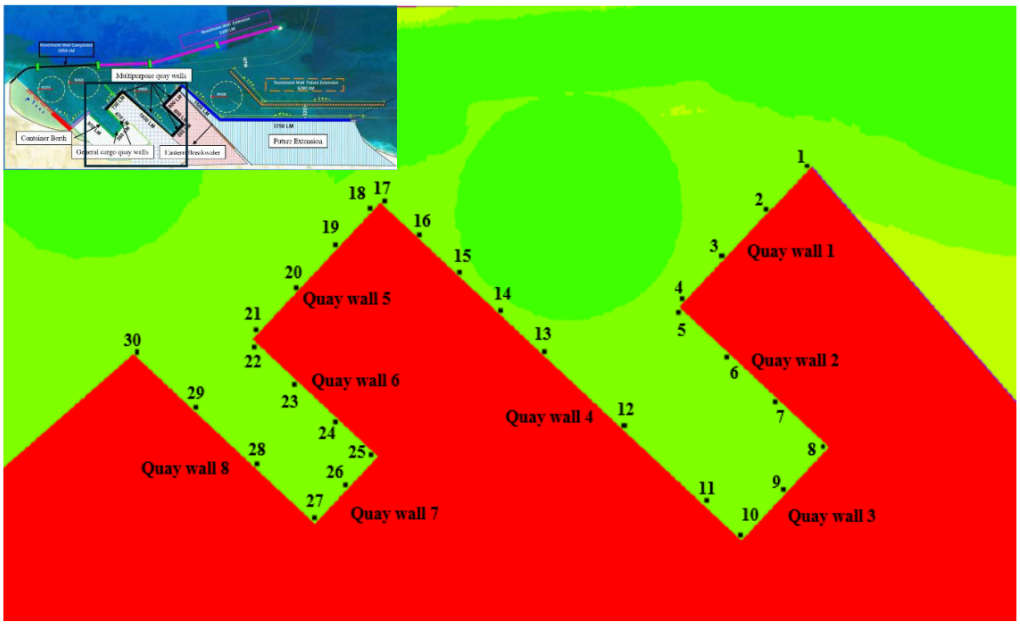

Figure 5. Locations of wave extraction points for operability assessment at Gargoub Port quay walls.

4.2.2. Downtime Assessment for Layout 1 (Current Development Stage)

The annual operational downtime of Gargoub Port under current and projected SLR conditions was evaluated using the 30-year SW hindcast (Tables 1–2), with the allowable Hs limits at each quay defined according to PIANC (2014). Bulk carriers and general cargo vessels were largely unaffected under both scenarios, with downtime ranging from 0 to 6.2 hr/yr at Quay 4 only. Container ships and Ro-Ro vessels were more sensitive to wave conditions, with the highest impacts at Multi-Purpose Quay 4, increasing modestly from 744.6 hr/yr under current water levels to 785.8 hr/yr under SLR. Quays 1 and 3 also experienced slight increases, from 545.8 to 593.9 hr/yr at Quay 1, and from 134 to 185.7 hr/yr at Quay 3. Quay 2 showed a moderate increase from 105.1 to 149.8 hr/yr, while Quay

5 and the other quay walls (General Cargo Quays 6–7 and Container Quay 8) remained largely unaffected. These results indicate that container and Ro-Ro operations at the more exposed multi-purpose quays already face significant operational constraints under current conditions, with SLR adding a small but noticeable increase in downtime, whereas bulk and general cargo operations remain largely reliable.

Table 6: Operational downtime (hr/yr) for different vessel types at Gargoub Port quay walls under current

Quay Wall Designation	Vessel Types	Hs Limit per PIANC [m]	Hm0/Hm0-incoming	Allowable Hm0-incoming[m]	Probability of Exceedance (%)	Downtime (hr/yr)
Multi-Purpose Quay 1	Bulk carriers Loading	1	0.30	3.33	0.00	0.00
	Bulk carriers Unloading	0.8		2.67	0.00	0.00
	General Cargo	0.8		2.67	0.00	0.00
	Container Ships	0.3		1.00	6.23	545.75
	RoRo Ships	0.3		1.00	6.23	545.75
Multi-Purpose Quay 2	Bulk carriers Loading	1	0.19	5.26	0.00	0.00
	Bulk carriers Unloading	0.8		4.21	0.00	0.00
	General Cargo	0.8		4.21	0.00	0.00
	Container Ships	0.3		1.58	1.20	105.12
	RoRo Ships	0.3		1.58	1.20	105.12
Multi-Purpose Quay 3	Bulk carriers Loading	1	0.20	5.00	0.00	0.00
	Bulk carriers Unloading	0.8		4.00	0.00	0.00
	General Cargo	0.8		4.00	0.00	0.00
	Container Ships	0.3		1.50	1.53	134.03
	RoRo Ships	0.3		1.50	1.53	134.03
Multi-Purpose Quay 4	Bulk carriers Loading	1	0.34	2.94	0.00	0.00
	Bulk carriers Unloading	0.8		2.35	0.01	0.79
	General Cargo	0.8		2.35	0.01	0.79
	Container Ships	0.3		0.88	8.50	744.60
	RoRo Ships	0.3		0.88	8.50	744.60
Multi-Purpose Quay 5	Bulk carriers Loading	1	0.10	10.00	0.00	0.00
	Bulk carriers Unloading	0.8		8.00	0.00	0.00
	General Cargo	0.8		8.00	0.00	0.00
	Container Ships	0.3		3.00	0.00	0.00
	RoRo Ships	0.3		3.00	0.00	0.00
General Cargo Quay 6	General Cargo	0.8	0.10	8.00	0.00	0.00
General Cargo Quay 7	General Cargo	0.8	0.09	8.89	0.00	0.00
Container Quay 8	Container Ships	0.3	0.10	3.00	0.00	0.00

Table 7: operational downtime (hr/yr) for different vessel types at Gargoub Port quay walls under projected

Quay Wall Designation	Vessel Types	Hs Limit per PIANC [m]	Hm0/Hm0-incoming	Allowable Hm0-incoming[m]	Probability of Exceedance (%)	Downtime (hr/yr)
Multi-Purpose Quay 1	Bulk carriers Loading	1	0.30	3.33	0.00	0.00
	Bulk carriers Unloading	0.8		2.67	0.00	0.00
	General Cargo	0.8		2.67	0.00	0.00
	Container Ships	0.3		1.00	6.78	593.93
	RoRo Ships	0.3		1.00	6.78	593.93
Multi-Purpose Quay 2	Bulk carriers Loading	1	0.19	5.26	0.00	0.00
	Bulk carriers Unloading	0.8		4.21	0.00	0.00
	General Cargo	0.8		4.21	0.00	0.00
	Container Ships	0.3		1.58	1.71	149.80
	RoRo Ships	0.3		1.58	1.71	149.80
Multi-Purpose Quay 3	Bulk carriers Loading	1	0.20	5.00	0.00	0.00
	Bulk carriers Unloading	0.8		4.00	0.00	0.00
	General Cargo	0.8		4.00	0.00	0.00
	Container Ships	0.3		1.50	2.12	185.71
	RoRo Ships	0.3		1.50	2.12	185.71
Multi-Purpose Quay 4	Bulk carriers Loading	1	0.34	2.94	0.00	0.00
	Bulk carriers Unloading	0.8		2.35	0.07	6.13
	General Cargo	0.8		2.35	0.07	6.13
	Container Ships	0.3		0.88	8.97	785.77
	RoRo Ships	0.3		0.88	8.97	785.77
Multi-Purpose Quay 5	Bulk carriers Loading	1	0.10	11.11	0.00	0.00
	Bulk carriers Unloading	0.8		8.89	0.00	0.00
	General Cargo	0.8		8.89	0.00	0.00
	Container Ships	0.3		3.33	0.00	0.00
	RoRo Ships	0.3		3.33	0.00	0.00
General Cargo Quay 6	General Cargo	0.8	0.10	8.00	0.00	0.00
General Cargo Quay 7	General Cargo	0.8	0.09	8.89	0.00	0.00
Container Quay 8	Container Ships	0.3	0.10	3.00	0.00	0.00

4.2.3. Downtime Assessment for Layout 2 (Final Planned Expansion)

The simulation results for the fully expanded Layout 2 demonstrate a dramatic improvement in port tranquility and overall operational stability. The construction of the northern and additional entrance breakwaters significantly enhances sheltering conditions for all berths, effectively mitigating the impact of incoming waves from offshore directions. For all vessel types, including those most sensitive to wave-induced motion, such as container and Ro-Ro ships, the calculated operational downtime is reduced to zero hr/yr under both baseline and projected sea-level rise (SLR) conditions. This indicates that Layout 2 provides nearly complete protection against operational disruptions caused by extreme wave events.

Quantitatively, the Hm0/Hm0_incoming ratios at the quay walls are drastically lower in Layout 2 compared to the interim Layout 1, reflecting the superior energy attenuation achieved by the completed breakwater system. These reductions in wave energy at berth locations translate directly to improved safety and efficiency during vessel berthing, cargo handling, and other port operations. Furthermore, as observed with Layout 1, the inclusion of the +1.01 m SLR scenario does not introduce any additional operational downtime, demonstrating the design's robustness to moderate sea-level projections.

The fully expanded layout not only satisfies operational criteria under current conditions but also provides a substantial factor of safety against future environmental changes. Its design ensures that port operations remain resilient even under upper-bound SLR scenarios, allowing the port to maintain uninterrupted service and protect sensitive vessel types from wave-induced delays. Overall, Layout 2 represents a comprehensive engineering solution, integrating hydrodynamic performance with operational reliability, and serves as a validated framework for resilient port planning in Mediterranean coastal environments.

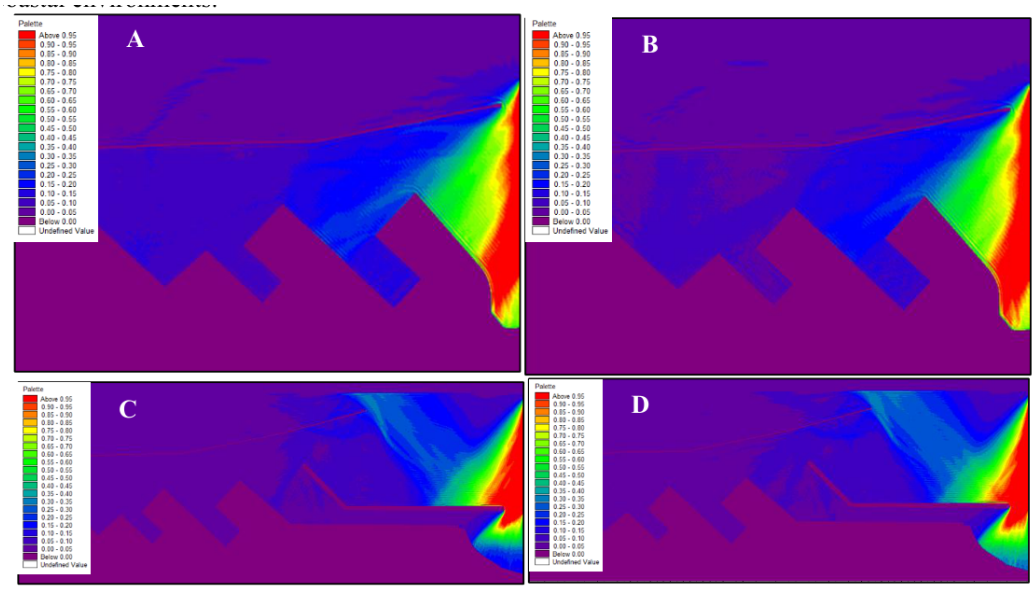

Figure 6. BW simulation results showing wave agitation at Gargoub Port: (A) Layout 1 – current water

Figure 6. BW simulation results showing wave agitation at Gargoub Port: (A) Layout 1 – current water levels, (B) Layout 1 – SLR scenario, (C) Layout 2 – normal water levels, (D) Layout 2 – SLR scenario.

4.2.4. Navigation Channel Shutdown Analysis

Beyond berth-level operability, the overall functionality of the port can be compromised when wave heights at the navigation channel entrance exceed the critical threshold established by Egyptian port authorities, set at 2.0 m (Romya et al., 2025). Such conditions trigger a full port shutdown, preventing all vessels from safely entering or exiting the harbor regardless of individual berth readiness. To assess the likelihood of these extreme events, the 30-year SW hindcast (1994–2024) was analyzed at the channel entrance located at 31°31′28.08″N, 26°39′4.40″E. The results indicate that waves exceeding the 2.0 m threshold are relatively rare but occur consistently throughout the hindcast period. Statistically, these exceedances account for approximately 3.89% of the time, which is equivalent to around 341 hours per year when the port would be effectively inoperable due to wave conditions. When considering projected SLR, climate shows only a marginal increase in severity, with the frequency of threshold exceedance rising slightly to 3.94%, corresponding to approximately 345 hours per year. This minimal increase demonstrates that even under future sea-level rise, the annual likelihood of full port closure at the

navigation channel remains essentially unchanged, highlighting that extreme wave events, rather than gradual water level rise, are the primary drivers of port-wide shutdown risk. These findings underscore the importance of incorporating both extreme wave statistics and long-term sea-level projections into operational planning and risk management for Gargoub Port, particularly for scheduling, emergency preparedness, and mitigation strategies.

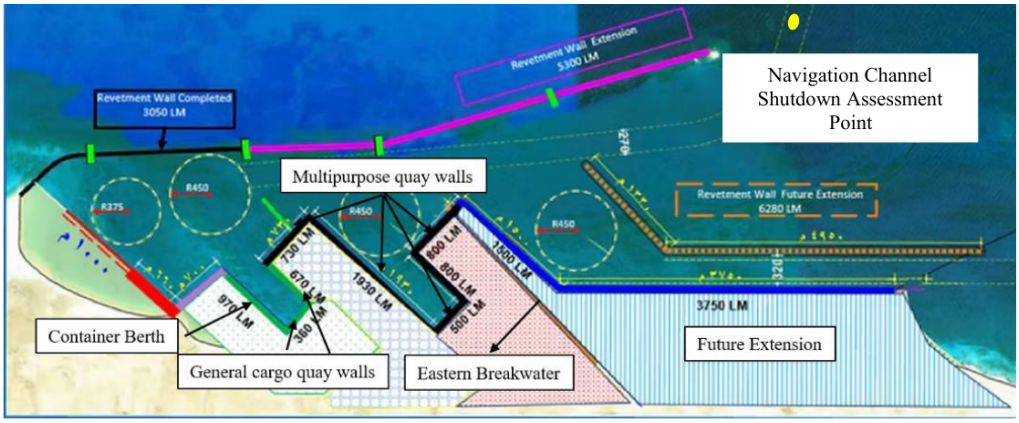

Figure 7. Navigation Channel Shutdown Assessment Point.

5. CONCLUSION AND RECOMMENDATIONS

This study has successfully quantified the significant risk of wave-induced operational downtime at Gargoub Commercial Port under both present-day and future sea-level conditions by implementing a coupled MIKE 21 Spectral and Boussinesq wave modeling framework. The analysis yields a critical comparative assessment of port layouts, revealing that the near-complete interim configuration (Layout 1) leaves key port operations highly vulnerable. Container and Ro-Ro vessels, in particular, face substantial annual disruptions, with downtime peaking at 745 hours per year at the exposed multi- purpose berths of quay 4, and extending to 546 hours at quay 1. While operations for bulk and general cargo at quays 2 (105 hr/yr) and 3 (134 hr/yr) are less affected, the cumulative impact on the port's core container and Ro-Ro services is pronounced. In stark contrast, the final planned expansion (Layout 2) demonstrates exceptional engineering efficacy, effectively eliminating berth-level downtime for all vessel types and thereby showcasing its inherent robustness and long-term operational resilience. A pivotal finding is that a projected sea-level rise of +1.01 m exerts only a minimal additional impact on berth operability, though it is crucial to note that full port shutdowns, dictated by hazardous conditions at the navigation channel entrance, remain considerable at approximately 341-345 hours annually under both current and future scenarios.

These findings carry direct and weighty implications for port management and planning. They underscore the paramount strategic importance of expediting the completion of Layout 2, which is essential for protecting operational reliability, especially for high-value container and Ro-Ro traffic

during the vulnerable interim construction period. In the interim Layout 1, proactive adjustments in vessel scheduling and assignment for the most exposed berths are strongly recommended to mitigate temporary operational and financial risks. Looking beyond immediate logistical concerns, this study establishes a foundation for several critical avenues of future research. Subsequent assessments should extend the applied framework to evaluate the performance of any newly planned berths, investigate potential

water quality issues by modeling flushing time within the expanded enclosed basin, and conduct a thorough economic analysis of the downtime costs quantified here. Furthermore, to ensure long-term climate resilience, future modeling must incorporate a wider suite of climate change projections, including intensified extreme storm events and more extreme sea-level rise scenarios beyond 2100.

In a broader context, this research provides a validated, replicable modeling framework that effectively bridges sophisticated hydrodynamic simulation with pragmatic port operational metrics, thereby offering a powerful decision-support tool for engineers and planners dedicated to resilient port infrastructure. By rigorously linking scientific analysis with real-world management priorities, the findings contribute to evidence-based, adaptive strategies for sustainable port development, especially in the Mediterranean region where ports are indispensable economic nodes yet increasingly vulnerable to natural and climatic hazards.

6. ACKNOWLEDGEMENT

The authors gratefully acknowledge Romya for providing wave data from his Northern Egyptian Wave Model (CoRI), which were essential for model calibration, and DHI for granting access to the MIKE Student Labkit license that facilitated the numerical modeling.

7. DECLARATION OF GENERATIVE AI AND AI-ASSISTED TECHNOLOGIES

The author(s) declare that no generative AI or AI-assisted tools were used during the preparation of this work.

8. REFERENCES

1. Alkhalidi, M., Al-Dabbous, A., Al-Dabbous, S., & Alzaid, D. (2025). Evaluating the accuracy of the ERA5 model in predicting wind speeds across coastal and offshore regions. Marine Sciences and Engineering, 13(149). https://doi.org/10.3390/jmse13010149
2. Al-Rammahi, A. M., & Al-Shukur, A.-H. K. (2025). Numerical simulation of hydrodynamic and spectral model of Iraqi coastal water at the northern Arabian Gulf. CFD Letters, 17(9). https://doi.org/10.37934/cfdl.17.9.194211
3. Becker, A. H., Acciaro, M., Asariotis, R., Cabrera, E., Cretegny, L., Crist, P., ... Velegrakis, A. (2013). A note on climate change adaptation for seaports: A challenge for global ports, a challenge for global society. Climate Change, 120(4), 683–695. https://doi.org/10.1007/s10584-013-0843-z
4. Copernicus Marine Data Store CMEMS. (2025). Mediterranean Sea physics reanalysis. https://data.marine.copernicus.eu/
5. DHI MIKE. (2025). MIKE 21 Spectral Waves FM, Spectral Wave Module User Guide. DHI MIKE (2025). MIKE 21 BW, Boussinesq Waves Module User Guide. Gandoin, R., & Garza, J. (2024). Underestimation of strong wind speeds offshore in ERA5: Evidence, discussion and correction. Wind Energy Science, 9(8), 1727–1745. https://doi.org/10.5194/wes-9-1727-2024
6. Google Earth. (2025). Gargoub Port, Egypt. https://earth.google.com/
7. Holthuijsen, L., Booij, N., & Herbers, T. (1989). A prediction model for stationary, short-crested waves in shallow water with ambient currents. Coastal Engineering, 13(1), 23–54. https://doi.org/10.1016/0378-3839(89)90031-8

8. Hzami, A., Heggy, E., Amrouni, O., Mahé, G., Maanan, M., & Abdeljaouad, S. (2021). Alarming coastal vulnerability of the deltaic and sandy beaches of North Africa. Scientific Reports, 11, 2320. https://doi.org/10.1038/s41598-020-77926-x
9. IPCC. (2021). Summary for policymakers. Climate change 2021: The physical science basis. Contribution of Working Group I to the Sixth Assessment Report of the Intergovernmental Panel on Climate Change. Cambridge: Cambridge University Press. https://doi.org/10.1017/9781009157896.001
10. Ji, W., Li, R., Xue, W., Cao, Z., Yang, H., Ning, Q., Hu, X., & Liao, G. (2025). Evaluation of ERA5 wind parameter with in-situ data offshore China. PLoS One, 20(5). https://doi.org/10.1371/journal.pone.0317751
11. Jebbad, R., Sierra, J. P., Mösso, C., Mestres, M., & Sánchez-Arcilla, A. (2022). Assessment of harbour inoperability and adaptation cost due to sea level rise: Application to the port of Tangier-Med (Morocco). Applied Geography, 138. https://doi.org/10.1016/j.apgeog.2021.102623
12. Kamel, O., Mostafa, T., Soliman, A., & El-Tahhan, M. (2025). Optimizing the draft of a quay wall to the anchor length ratio using finite element numerical model. In The International Maritime Transport and Logistics (MARLOG 14): Artificial Intelligence Implementations Towards Shaping the Future of Digital World. Alexandria, Egypt.
13. Mamdouh, A., Elgendi, E. O., Soliman, A., & Shehata, A. S. (2024). Energy management optimization based on facilities layout planning for port construction: Mediterranean region case study. In The International Maritime and Logistics Conference (MARLOG 13): Towards Smart Green Blue Infrastructure. Alexandria, Egypt.
14. Maritime Transport & Logistics Sector, Arab Republic of Egypt. (2025, October 15). A boom in Egyptian ports: Achievement that redraw Red Sea and Mediterranean map. https://www.mts.gov.eg/en/
15. Maritime Transport & Logistics Sector, Arab Republic of Egypt. (2025). Gargoub. https://www.mts.gov.eg/ar/port/جرجوب/
16. Michel, M., Soliman, A., & Shehata, A. S. (2024). Assessment of renewable energy supply for shore side electricity in green ports. In The International Maritime and Logistics Conference (MARLOG 13): Towards Smart Green Blue Infrastructure. Alexandria, Egypt.
17. PIANC. (2014). Report No. 121: Harbour approach channels design guidelines. Romya, A. A., Elkut, A. E., AbuZed, A. A., Moghazy, H. M., El-Tahhan, M. K., Soliman, A., ... Sharaan, M. (2025). Adaptation and development plans of the Egyptian ports under the impacts of climate change. Ocean and Coastal Management, 262. https://doi.org/10.1016/j.ocecoaman.2025.107577
18. Samaras, A. G., Gaeta, M. G., Miquel, A. M., & Archetti, R. (2016). High-resolution wave and hydrodynamics modelling in coastal areas: Operational applications for coastal planning, decision support and assessment. Natural Hazards and Earth System Sciences, 16, 1499–1518. https://doi.org/10.5194/nhess-16-1499-2016
19. Sierra, J., Casanovas, I., Mösso, C., Mestres, M., & Sánchez-Arcilla, A. (2016). Vulnerability of Catalan (NW Mediterranean) ports to wave overtopping due to different scenarios of sea level rise. Regional Environmental Change, 16(5), 1457–1468. https://doi.org/10.1007/s10113-015-0879-x
20. Sierra, J., Casas-Prat, M., Virgili, M., Mösso, C., & Sánchez-Arcilla, A. (2015). Impacts on wave- driven harbour agitation due to climate change in Catalan ports. Natural Hazards and Earth System Sciences, 15(8), 1695–1709. https://doi.org/10.5194/nhess-15-1695-2015
21. Sierra, J., Genius, A., Lionello, P., Mestres, M., Mösso, C., & Marzo, L. (2017). Modelling the impact of climate change on harbour operability: The Barcelona port case study. Ocean Engineering, 141, 64–78. https://doi.org/10.1016/j.oceaneng.2017.06.002
22. Sierra, J., Sánchez-Arcilla, A., Gironella, X., Gracia, V., Altomare, C., Mösso, C., ... Barahona, C. (2023). Impact of climate change on berthing areas in ports of the Balearic Islands: Adaptation measures. Frontiers in Marine Science, 10. https://doi.org/10.3389/fmars.2023.1124763